

Molecular States in Carbon Nanotube Double Quantum Dots

M. R. Gräber, W. A. Coish, C. Hoffmann[§], M. Weiss, J. Furer, S. Oberholzer, D. Loss, and C. Schönenberger^{*}

Institut für Physik, Universität Basel, Klingelbergstr. 82, CH-4056 Basel, Switzerland

(Dated: April 4, 2018)

We report electrical transport measurements through a semiconducting single-walled carbon nanotube (SWNT) with three additional top-gates. At low temperatures the system acts as a double quantum dot with large inter-dot tunnel coupling allowing for the observation of tunnel-coupled molecular states extending over the whole double-dot system. We precisely extract the tunnel coupling and identify the molecular states by the sequential-tunneling line shape of the resonances in differential conductance.

PACS numbers: 73.63.-b, 73.23.-b, 03.67.-a

The interference of quantum states is one of the most striking features of nature enabling the formation of molecular bonds. This bond formation can be studied in coupled quantum dots (artificial molecules) in regimes that are not accessible in true molecules [1, 2, 3, 4, 5]. Additionally, these engineered artificial molecules have been proposed as logic elements for future applications in spin-based quantum computing [6]. Whereas most electrical transport experiments on coupled quantum dots so far have investigated GaAs-based semiconductor quantum dots (see [7] and references therein), only recently such structures have been realized in carbon nanotubes and semiconducting nanowires [8, 9]. These materials are attractive not just for the relative ease in production, but also for the fact that superconducting and ferromagnetic contacts have been demonstrated [10, 11, 12], opening up a road for various kinds of novel quantum devices [13]. In addition, large spin dephasing times are expected for carbon-based quantum dots, since the nuclear spin of the dominant isotope ^{12}C is zero, yielding a strongly reduced hyperfine interaction.

In this letter, we report electrical transport measurements through a semiconducting single-walled carbon nanotube (SWNT) with source and drain electrodes and three additional top-gates. In specific gate-voltage ranges the system acts as a double quantum dot with *large* inter-dot tunnel coupling t , allowing for the observation of a quantum-mechanical superposition of $|n, m+1\rangle$ and $|n+1, m\rangle$ states where n and m denote the number of charges on the left and right dot, respectively. Using an effective single-particle picture, we precisely determine the tunnel coupling and identify molecular-like states with wave functions extending over the whole nanotube double dot.

Single-walled carbon nanotubes were grown by means of chemical vapor deposition (for details see Ref. [14]) on a highly-doped Si substrate covered by an insulating layer of 400 nm SiO_2 . Single nanotubes were selected using a scanning electron microscope. Three 200 nm wide local gates equally spaced by 400 nm were then defined by means of standard electron beam lithography and e-gun evaporation of SiO_2 , Ti and Pd. Finally, Pd source

and drain contacts were fabricated. Figure 1(a) shows a schematic of the device, the materials used, and corresponding film thicknesses. A scanning electron micrograph of a device is shown in Fig. 1(b).

Room temperature characterization identifies the semiconducting nature and an intrinsic p-doping state of the nanotube. Figure 1(c) shows the linear conductance through the device as a function of the three top-gate voltages. At a top-gate voltage of roughly 0.4 V conductance is suppressed indicating that the chemical potential is shifted into the semiconducting gap of the tube. Five identically-prepared devices were tested at room temperature and showed the same behavior.

Low-temperature measurements were performed in a ^3He cryostat with a base temperature of 290 mK. Differential conductance dI/dV_{sd} was measured using stan-

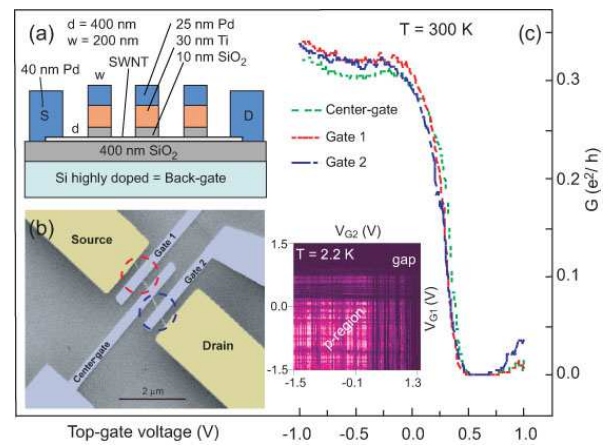


FIG. 1: (a) Schematic of the fabricated device, with three top-gates as labelled in (b). (b) Scanning electron micrograph of a sample fabricated identically to the one measured. The distance from source to drain is $2.2\ \mu\text{m}$. Dashed circles denote the regions affected by gates 1 and 2. (c) Conductance G through the device at $T = 300\text{ K}$ versus top-gate voltage. All gates not swept are connected to ground. Note: Differences between the individual gate scans at 0 V arise from slightly hysteretic gate responses. Inset: Colorscale plot of G versus gate 1 and gate 2 for fixed $V_C = -1\text{ V}$ at 2.2 K . Bright corresponds to $0.4\text{ e}^2/\text{h}$, dark to $0\text{ e}^2/\text{h}$.

dard lock-in techniques with an excitation voltage of typically $7.5 \mu\text{V}$ at a frequency of 327.7 Hz and an I/V converter with a gain of 10^7 V/A . The inset of Fig. 1(c) shows a colorscale plot of the linear conductance versus voltages applied at gates 1 and 2 for a constant center gate voltage $V_C = -1 \text{ V}$ at 2.2 K . Again, applying positive voltages of the order 1 V to any of the top-gates locally shifts the chemical potential into the energy gap of the intrinsically p-doped SWNT and thus suppresses electrical transport. Additionally, sweeping gate 1 and gate 2 leads to pronounced oscillations of the conductance due to single-electron charging and finite-size effects of the nanotube, which are accessible at low temperatures. For the measurements presented in the following, the center and back-gate were kept at constant voltages $V_C = -0.1 \text{ V}$, $V_{BG} = 0 \text{ V}$, respectively, and no magnetic field was applied.

A magnified colorscale plot of the differential conductance dI/dV_{sd} in a reduced gate-voltage range is shown in Fig. 2(a). The visible high-conductance ridges define a charge-stability map that is shaped like a honeycomb. This honeycomb pattern is characteristic of a double quantum dot. Within each cell, the number of holes (n, m) on the two dots is constant. Energizing gate 1 (2) to more negative voltages successively fills holes into dot 1 (2), whereas a more positive voltage pushes holes out of the dot. Two identical devices were measured at low temperatures and both exhibited a similar honeycomb pattern.

Of particular importance for sequential tunneling through the double dot are the so-called triple points, the two blue points in Fig. 2(a), for example. At these points, three charge states are simultaneously degenerate (e.g. (n, m) , $(n + 1, m)$, and $(n, m + 1)$), enabling the shuttling of a single electron from source to drain through the two dots. The conductivity in the vicinity of a triple point strongly depends on the relative magnitude of the electrostatic and tunnel coupling. For purely electrostatic coupling, the triple points are sharply defined, while they become blurred, leading to curved edges, if quantum-mechanical tunneling is turned on.

We will first analyze the honeycomb pattern, assuming purely electrostatic interaction as illustrated in Fig. 2(d). Hence, we disregard the tunnel coupling between the dots for the moment. In the quantitative determination of the dot and gate capacitances, we follow the work of van der Wiel *et al* [7]. From the dimensions of a single cell $\Delta V_{G1,2} = |e|/C_{G1,2}$ as illustrated in Fig. 2(b), one obtains the gate capacitances $C_{G1} = 23 \text{ aF}$ and $C_{G2} = 21 \text{ aF}$. Applying a finite source-drain bias voltage V_{sd} results in a broadening of the triple points at the honeycomb edges into triangular-shaped regions, see Fig. 2(c). In our device the triangles are less clearly defined due to finite temperature and the strong tunnel coupling between the dots which we will discuss in the following paragraphs. Using the relation $C_{G1,2}/C_{1,2} =$

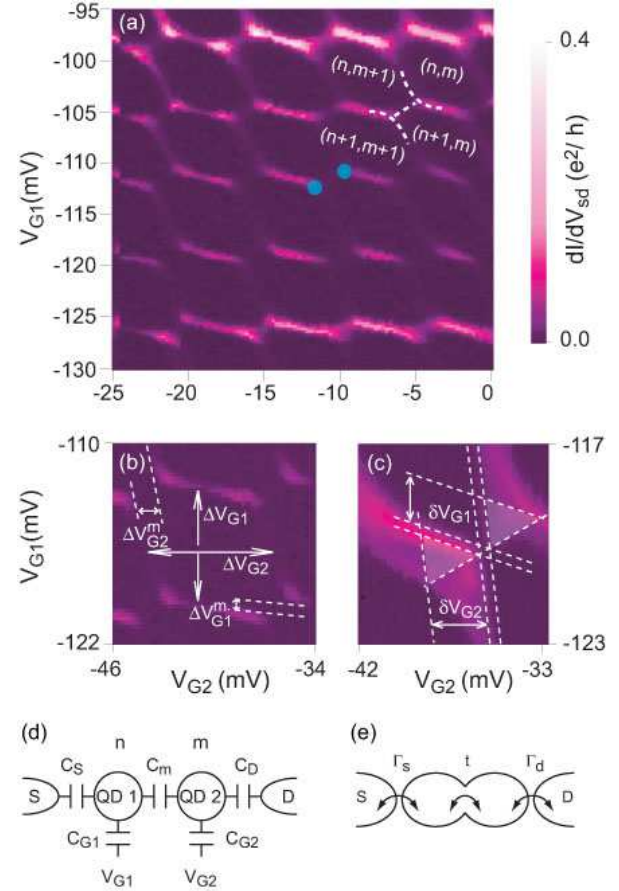


FIG. 2: (a) Colorscale plot of the conductance versus voltage applied on gate 1 (V_{G1}) and gate 2 (V_{G2}) at a temperature of $T = 290 \text{ mK}$ and $V_{sd} = -128 \mu\text{V}$. The resulting honeycomb pattern represents the charge stability diagram of coupled double quantum dots. Two triple points are marked by blue dots for clarity. Dashed lines are guides to the eye. (b) Close-up of a single honeycomb cell. (c) Vicinity of the triple points at a source-drain bias voltage of $391 \mu\text{V}$. (d) and (e) Capacitive and molecular model of a double quantum dot, respectively.

$|V_{sd}|/\delta V_{G1,2}$, the capacitances $C_1 = C_S + C_{G1} + C_m$ and $C_2 = C_D + C_{G2} + C_m$ follow to be 84 aF and 145 aF , respectively, from which we obtain $U_{C_{1,2}} = e^2/C_{1,2} \approx 1.9 \text{ meV}$ and 1.1 meV for the on-site charging energies of the dots, in agreement with the dimensions of the Coulomb blockade diamonds at finite bias (not shown). The mutual capacitance C_m between the two dots can now be estimated from the triple-point spacing $\Delta V_{G1,2}^m$ in Fig. 2(b) using $\Delta V_{G1,2}^m = |e|C_m/C_{G1,2}C_{2,1}$. We obtain $C_m \approx 15 \text{ aF}$.

We emphasize that disregarding tunneling between the dots is a very strong assumption. The purely electrostatic model, which we have used up to now, overestimates C_m and can only yield an upper bound. That tunneling is appreciable in this double-dot system is evidenced by the honeycomb borders in Fig. 2(a), which are bright over an

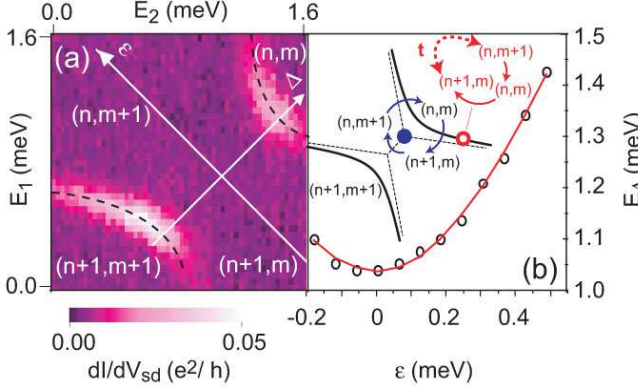


FIG. 3: (a) Colorscale plot of the differential conductance ($V_{sd} = 20 \mu\text{V}$, $T = 290 \text{ mK}$) in the vicinity of two triple points. Dashed lines are guides to the eye. (b) Spacing E_{Δ} (see Eq. (2)) of the two high conductance wings with respect to the Δ -direction versus detuning ϵ . Inset: Schematics of sequential tunnel processes allowed at the triple points (blue dot) and at the honeycomb edges (red circle) via molecular states.

extended range. In addition, the high-conductance ridges are *curved* in the vicinity of the triple points, as expected for strongly tunnel-coupled dots. Analyzing this curvature allows us to precisely extract the tunnel coupling amplitude t (see Fig. 3). To do so, a convenient description is developed first.

We adopt a model Hamiltonian of the form $H = H_C + H_T + H_L$, describing the system depicted in Fig. 2(e). Here, H_C describes the orbital and Coulomb energies of the double-dot system, $H_T = t(|n+1,m\rangle\langle n,m+1| + \text{h.c.})$ the tunnel-coupling between the two dots, and H_L the coupling of each dot to the leads. In H_C , we include on-site (U) and nearest-neighbor (U') charging energies. States with a fixed number of charges on each dot are eigenstates of H_C : $H_C|n,m\rangle = E_{nm}|n,m\rangle$, where $E_{nm} = E_{nm}^{\text{orb}} + \frac{U}{2}[n(n-1) + m(m-1)] + U'nm + E_{1n} + E_{2m}$. E_{nm}^{orb} is the total orbital energy of the $|n,m\rangle$ charge configuration, and $E_{1(2)}$ is the single-particle energy of the left (right) dot, supplied by the gate voltages $V_{G1,2}$. In a simple picture of sequential tunneling [15, 16] through H_C -eigenstates (neglecting H_T to leading order), one would expect nonzero conductance only at the triple points. It is only at these points that energy-conserving processes of the kind $|n,m\rangle \rightarrow |n+1,m\rangle \rightarrow |n,m+1\rangle \rightarrow |n,m\rangle$ can lead to charge transport through the double dot (blue sequence in the inset of Fig. 3(b)).

However, if we allow for superposed double-dot states of the form $|E\rangle = \alpha|n+1,m\rangle + \beta|n,m+1\rangle$, sequential transport is possible along the honeycomb edges as well (red sequence in the inset of Fig. 3(b)). Such superposed states are eigenstates of the full double-dot Hamiltonian $H_C + H_T$. For spinless holes [17] and assuming that only a single eigenstate $|E\rangle$ participates in transport, the sta-

tionary sequential-tunneling current is then given by

$$I = |e| \Gamma [f_s(\mu_{2dot}) - f_d(\mu_{2dot})]. \quad (1)$$

Here, $f_l(\mu_{2dot}) = 1/(\exp[(\mu_{2dot} - \mu_l)/kT] + 1)$ is a Fermi function at temperature T , μ_l ($l = s(d)$) the chemical potential of the source (drain) lead, and $\Gamma = |\alpha\beta|^2\Gamma_s\Gamma_d/(\alpha^2\Gamma_s + \beta^2\Gamma_d)$, with $\Gamma_{s(d)}$ the dot-lead tunneling rate to the source (drain). The chemical potential of the double dot μ_{2dot} depends on whether sequential tunneling occurs at $|n,m\rangle \leftrightarrow |E\rangle$ (right branch in the inset of Fig. 3(b)), or at $|n+1,m+1\rangle \leftrightarrow |E\rangle$ (left branch): $\mu_{2dot} = E - E_{nm}$ for the former and $E_{n+1,m+1} - E$ for the latter.

With the help of Eq. (1), the data allow for a precise quantitative analysis of the tunnel coupling t between the dots. Figure 3(a) shows a colorscale plot (linear scale) of the differential conductance at $V_{sd} = 20 \mu\text{V} \approx kT$ in the vicinity of a triple point region. As expected in the presence of tunnel-coupled eigenstates, transport is possible not only at the triple points, but also on the wings extending from the triple points. The two gate voltages V_{G1} and V_{G2} are converted into energies E_1 and E_2 by multiplying them with the conversion factors $\alpha_1 = 0.42e$ and $\alpha_2 = 0.29e$, which we obtain from the splitting of a differential conductance resonance at finite bias voltage, as will be discussed in the context of Fig. 4. We then change variables to $\epsilon = (E_1 - E_2)/\sqrt{2}$ and $\Delta = (E_1 + E_2)/\sqrt{2}$. In terms of these new variables, the double-dot molecular eigenenergies are (up to a constant offset) $E^{\pm}(\Delta, \epsilon) = E_{mn}(\Delta, \epsilon) + (\Delta \mp \sqrt{\epsilon^2 + 2t^2})/\sqrt{2}$. When the bias and temperature are smaller than the double-dot level spacing (i.e., $V_{sd}, kT < E^- - E^+$), transport occurs only through the ground-state $|E^+\rangle$. For small bias, we set $\mu_1 = \mu_2 = \mu$, then transport is due to energy-conserving transitions between the state $|E^+\rangle$ and either $|n,m\rangle$ (when $E^+ - E_{nm} = \mu$) or $|n+1,m+1\rangle$ (when $E_{n+1,m+1} - E^+ = \mu$). These conditions are fulfilled at the two high-conductance wings. The separation of the wings in the Δ -direction (E_{Δ}) is given by:

$$E_{\Delta} = \sqrt{2}U' + \sqrt{4\epsilon^2 + 8t^2}. \quad (2)$$

In Fig. 3(b) the spacing of the two wings E_{Δ} is plotted versus the detuning ϵ and fit to Eq. (2). Satisfactory fits to the data yield a tunnel coupling of $t = 310 \dots 360 \mu\text{eV}$ and $U' < 100 \mu\text{eV}$. The parameters of the fit shown are $t = 358 \mu\text{eV}$ and $U' = 16 \mu\text{eV}$. The relative magnitudes are compared as $2t \approx 0.7 \text{ meV} \gg U' < 0.1 \text{ meV}$. The fact that the tunnel coupling dominates by almost an order of magnitude over the electrostatic coupling between the dots reflects the one-dimensional geometry of a nanotube; electrostatic interactions are reduced due to the large separation of the "center of mass" of the charges (while still allowing a significant overlap of the wavefunctions). Similar molecular states have been analyzed in semiconductor vertical-lateral double dots, yielding a smaller tunnel

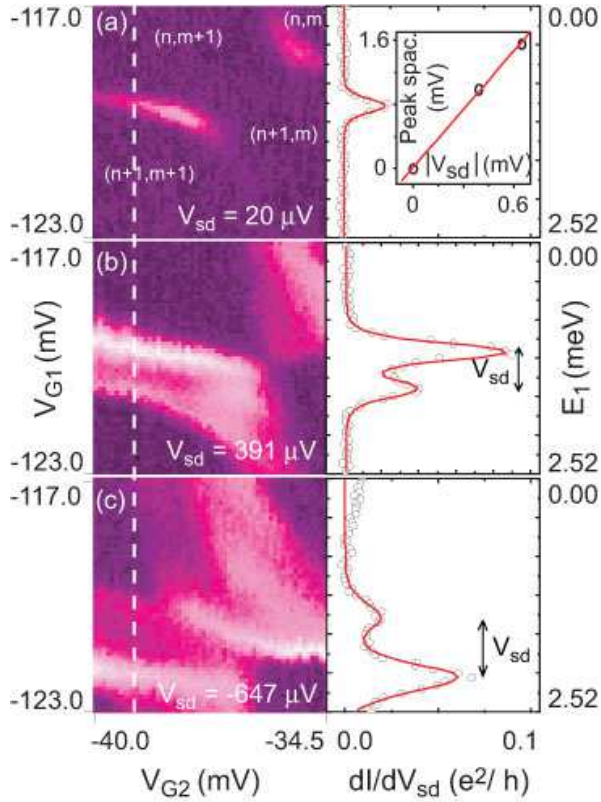


FIG. 4: Colorscale plot of the differential conductance in the vicinity of the same triple point as in Fig. 3 for three different bias voltage: (a) $V_{sd} = 20 \mu\text{V}$, (b) $V_{sd} = 391 \mu\text{V}$ and (c) $V_{sd} = -647 \mu\text{V}$. Dark corresponds to $0 e^2/h$ and bright to $0.1 e^2/h$. On the right side, open circles denote traces of the differential conductance taken at the position of the dashed line. Solid lines represent fits to the line shape given by Eq. (3). Left-hand vertical scale: Voltage applied to gate 1. Right-hand vertical scale: Voltage applied to gate 1 converted into energy.

coupling $t \approx 80 \mu\text{eV}$ and larger $U' \approx 175 \mu\text{eV}$ [18]. Using $U' < 100 \mu\text{eV}$ and $U' = \frac{2e^2C_m}{C_1C_2-C_m^2}$ [19], one obtains a mutual capacitance of $C_m \lesssim 4 \text{ aF}$, consistent with the previous estimate $C_m \leq 15 \text{ aF}$ from the purely electrostatic model.

Because $t \gg kT$ at $T = 0.3 \text{ K}$, charge transport in the vicinity of the triple points takes place through a single molecular orbital (the bonding orbital of the two dots). This can be distinguished from two-stage hopping if dI/dV_{sd} is further analyzed as a function of bias voltage. More specifically, we demonstrate next that the finite-bias differential conductance through the double dot is accurately described by the sequential tunneling through a single molecular state according to Eq. (1).

Figure 4 shows a map of the differential conductance in the vicinity of the two triple points (same region as Fig. 3) for three different source-drain voltages. On the right side, traces of the differential conductance with respect to gate 1 are extracted for fixed voltage applied

to gate 2 (dashed line), well separated from the triple points. In Fig. 4(a) the conductance trace has a single peak. In the finite-bias cases (b) and (c) the single peak splits into two peaks. Because of the linear dependence of the peak splitting on bias (inset of Fig. 4(a) for gate 1), the second peak is not due to an additional level entering the bias window. To understand this feature, we note that the differential conductance is measured by modulating the source voltage μ_1 , keeping the drain voltage μ_2 and all other gate voltages fixed. Assuming the double-dot charge is fixed, capacitive coupling of the source to the double dot induces a simultaneous modulation of μ_{2dot} , albeit with an amplitude reduced by the factor $r = \partial\mu_{2dot}/\partial\mu_1 = C_S/C_\Sigma$, where $C_\Sigma \approx C_S + C_D + C_{G1} + C_{G2}$. From Eq. (1) the differential conductance for our setup is then given by

$$\frac{dI}{d\mu_1} = -|e|\Gamma[(1-r)f'_s(\mu_{2dot}) + rf'_d(\mu_{2dot})], \quad (3)$$

where $f'_l(x) = \frac{d}{dx}f_l(x)$. Sequential tunneling through a single molecular level therefore predicts a double-peaked structure with *peaks separated by the bias voltage*, as observed in Fig. 4. The spacing of the two peaks can thus be used to convert top-gate voltages into energy and one obtains the conversion factors given above. For our device, we have $C_S \approx 65 \text{ aF}$, $C_\Sigma \approx 230 \text{ aF}$, which yields $r \approx 0.3$. According to this model the relative height of the two differential conductance peaks should be roughly $\frac{r}{1-r} \approx 0.5$. This value is consistent with the data shown in Fig. 4 (with ratios of 0.42 in (b) and 0.28 in (c)). Additionally, we find that the asymmetry of the peaks switches from positive (b) to negative (c) bias, as is expected from Eq. (3).

The data in Fig. 4(a) have been fit to Eq. (3) yielding a peak width of $49 \mu\text{eV}$. Note that in this case $V_{sd} \approx kT$ and the peak thus does not split. Subtracting the bias of $20 \mu\text{V}$ one obtains an effective temperature of the electrons of $29 \mu\text{eV} \approx 335 \text{ mK}$. Fitting Fig. 4(b) and 4(c) to Eq. (3), one obtains a larger peak width corresponding to temperatures of 785 mK and 1180 mK , respectively, which we attribute to Joule heating at finite bias.

The excellent agreement of the sequential-tunneling fits demonstrates that transport occurs through a single level. In this regime of a strongly tunnel-coupled double dot, transport cannot be captured by dot-to-dot hopping, but takes root in the formation of coherent molecular states.

For assistance and discussions we thank W. Belzig, E. Bieri, C. Bruder, A. Eichler, V. N. Golovach, L. Grütter, G. Gunnarson, D. Keller, T. Kontos, S. Sahoo, and J. Gobrecht for oxidized Si-substrates. We acknowledge financial support from the Swiss NFS, the NCCR on Nanoscience, DARPA (WAC and DL), NSERC (WAC), and the ‘C. und H. Dreyfus Stipendium’ (MRG).

* Electronic address: christian.schoenenberger@unibas.ch
 [§] Present address: Université Joseph Fourier and CNRS / CRTBT, 25 av. des Martyrs, 38042 Grenoble, France
 [1] C. Livermore, C.H. Crouch, R.M. Westervelt, K.L. Campman, and A.C. Gossard, *Science* **274**, 1332 (1996).
 [2] R. H. Blick, D. Pfannkuche, R. J. Haug, K. v. Klitzing, and K. Eberl, *Phys. Rev. Lett.* **80**, 4032 (1997).
 [3] A. W. Holleitner, R. H. Blick, A. K. Hüttel, K. Eberl, and J. P. Kotthaus, *Science* **297**, 70 (2002).
 [4] J.M. Elzermann, R. Hanson, J.S. Greidanus, L.H. Willems van Beveren, S. De Franceschi, L.M.K. Vandersypen, S. Tarucha, and L.P. Kouwenhoven, *Phys. Rev. B* **67**, 161308 (2003).
 [5] J. R. Petta, A. C. Johnson, J. M. Taylor, E. A. Laird, A. Yacoby, M. D. Lukin, C. M. Marcus, M. P. Hanson, and A. C. Gossard, *Science* **309**, 2180 (2005).
 [6] G. Burkard, D. Loss, and D. P. DiVincenzo, *Phys. Rev. B* **59**, 2070 (1999).
 [7] W. G. van der Wiel, S. de Franceschi, J. M. Elzermann, T. Fujisawa, S. Tarucha and L. P. Kouwenhoven, *Rev. Mod. Phys.* **75**, (2003).
 [8] N. Mason, M. J. Biercuk, and C. M. Marcus, *Science* **303**, 655 (2004); M. J. Biercuk, S. Garaj, N. Mason, J. M. Chow, and C. M. Marcus, *Nano Letters*, **5**, 1267

(2005).
 [9] C. Fasth, A. Fuhrer, M. Björk, and L. Samuelson, *Nano Letters* **5**, 1487 (2005).
 [10] M. R. Buitelaar, T. Nussbaumer, and C. Schönenberger, *Phys. Rev. Lett.* **89**, 256801 (2002).
 [11] Y.-J. Doh, J. A. van Dam, A. L. Roest, E. P. A. M. Bakkers, L. P. Kouwenhoven, and S. De Franceschi, *Science* **309**, 272 (2005).
 [12] S. Sahoo, T. Kontos, J. Furer, C. Hoffmann, M. Gräber, A. Cottet, and C. Schönenberger, *Nature Physics* **1**, 99 (2005).
 [13] M.-S. Choi, C. Bruder, and D. Loss, *Phys. Rev. B* **62**, 13569 (2000).
 [14] J. Furer, PhD Thesis, University of Basel, (2005).
 [15] We define a sequential-tunneling process for the double dot as a process that changes the total charge on the double-dot by one, as in Ref. [16].
 [16] V.N. Golovach, and D. Loss, *Phys. Rev. B* **69**, 245327 (2004).
 [17] Note that in a spinless description we exclude the possibility of e.g. spin-blockade, which, in our experiment, has not been observed.
 [18] T. Hatano, M. Stopa, and S. Tarucha, *Science* **309**, 268 (2005).
 [19] R. Ziegler, C. Bruder, and H. Schoeller, *Phys. Rev. B* **62**, 1961 (2000).